Inorganic Chemistry

Article

pubs.acs.org/IC

Peri-Substituted Phosphorus–Tellurium Systems–An Experimental and Theoretical Investigation of the P···Te through-Space Interaction

Andreas Nordheider,[†] Emanuel Hupf,[‡] Brian A. Chalmers,[†] Fergus R. Knight,[†] Michael Bühl,[†] Stefan Mebs,[§] Lilianna Chęcińska,[∥] Enno Lork,[‡] Paula Sanz Camacho,[†] Sharon E. Ashbrook,[†] Kasun S. Athukorala Arachchige,[†] David B. Cordes,[†] Alexandra M. Z. Slawin,[†] Jens Beckmann,*[,‡] and J. Derek Woollins*[,†]

[†]EaStChem School of Chemistry, University of St. Andrews, Fife KY16 9ST, St Andrews, U.K.

[‡]Institut für Anorganische Chemie, Universität Bremen, Leobener Straße, 28359 Bremen, Germany

[§]Institut für Chemie und Biochemie, Freie Universität Berlin, Fabeckstraße 36a, 14195 Berlin, Germany

[∥]Department of Theoretical and Structural Chemistry, University of Lodz, Pomorska 163/165, 90-236 Lodz, Poland

Supporting Information

ABSTRACT: A series of *peri*-substituted phosphorus–tellurium systems R′Te–Acenap–PR_2 (R′ = Ph, *p*-An, Nap, Mes, Tip; Acenap = acenaphthene-5,6-diyl ($-C_{12}H_8$); R = ^{i}Pr, Ph) exhibiting large "through-space" spin–spin coupling constants and the "onset" of three-center four-electron type interactions is presented. The influence of the substituents at the phosphorus and tellurium atoms as well as their behavior upon oxidation (with S, Se) or metal-coordination (Pt, Au) is discussed using NMR spectroscopy, single-crystal X-ray diffraction, and advanced density functional theory studies including NBO, AIM, and ELI-D analyses.

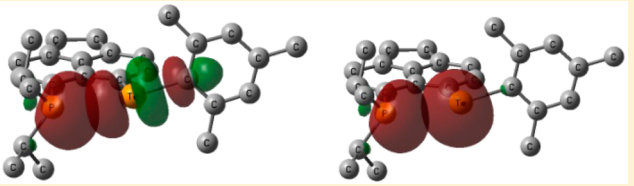

INTRODUCTION

Peri-substitution has proven to be a powerful tool in the investigation of unusual bonding situations and interactions between two or more atoms through space (e.g., through-space spin–spin coupling). The rigid naphthalene or acenaphthene backbone is responsible for a special situation in which the two *peri*-substituted atoms are forced into sub-van der Waals contacts, resulting in significant interactions that favor the formation of unusual systems, often with unique properties (Figure 1).[1−4]

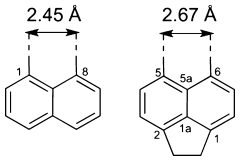

Figure 1. *Peri*-substitution in naphthalene and acenaphthene can force two elements into sub-van der Waals distances.

These systems include highly basic 1,8-*N*,*N*-substituted naphthalenes acting as "proton sponge" compounds (Figure 2A),[5] a P^{III}–P^{III} species with a rare σ^3P–σ^3P bonding (Figure 2B),[6] a P^{III}–P^{V} system with an unusual σ^4P–σ^6P bonding interaction (Figure 2C),[7] a hypercoordinated P–P system showing a frozen early stage of nucleophile–electrophile interaction (Figure 2D),[8] different structure types in group 15 phosphorus-element dichlorides (Figure 2E,F),[9−11] thermally stable cyclic phosphanylidene-σ^4-phosphorane[12] and an arsanylidene-σ^4-phosphorane (Figure 2G),[10] or a 1,2-ditellura-acenaphthene-1,2-dication (Figure 2H).[13]

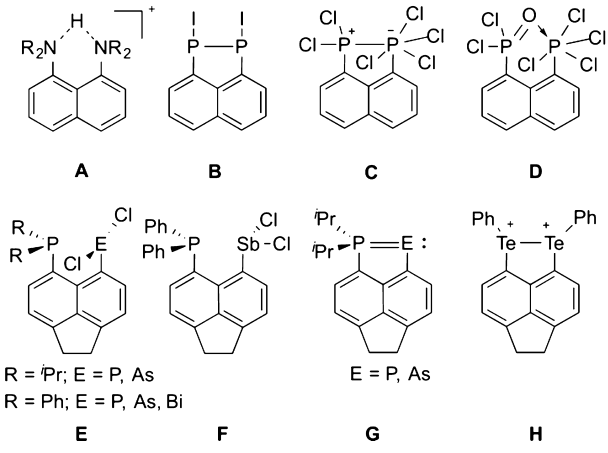

Figure 2. Examples of unusual bonding situations realized through *peri*-substitution.

Known examples of *peri*-substituted phosphorus-chalcogen systems (P–E; E = S, Se, Te) include sulfur and selenium species. The selenium compounds RSe–Nap–PPh_2, which are stabilized by a naphthalene backbone, exhibit large P···Se

Received: December 22, 2014
Published: February 18, 2015

DOI: 10.1021/ic503056z
Inorg. Chem. 2015, 54, 2435−2446

interactions between two or more atoms not directly linked by covalent bonds (e.g., through-space spin−spin coupling).[14,15]

Stable phosphorus−tellurium species are a very limited class of compounds, and only few examples of these have been reported to date,[16−19] whereas no *peri*-substituted P,Te systems have been described yet. The study of such *peri*-substituted systems could prove to be a valuable tool in developing a better understanding of phosphorus−tellurium chemistry including through-space interactions between these two elements. On this note, the present work demonstrates the first series of *peri*-substituted P,Te systems and a discussion of the nature of the interactions, the influence of substitution, and the reason for unusual P−Te spin−spin coupling constants in these non- or weakly bonded systems.

1. RESULTS AND DISCUSSION

This section is organized into two subchapters concerning Te^{II}/P^{III} species **1**−**5** with an emphasis on through-space interactions between the phosphorus and tellurium atoms (part 1) and a second subchapter, which focuses on the influence of transformations (e.g., oxidation, complexation) on the through-space interaction.

1.1. Synthesis. The lithiation of R_2P−Acenap−Br[20] (Acenap = acenaphthene-5,6-diyl (−$C_{12}H_8$)) with ^{n}BuLi (TMEDA) and subsequent reaction with different monotelluride iodides yielded a series of *peri*-substituted P,Te compounds **1**−**5** that offer intriguing properties for ^{31}P and ^{125}Te NMR studies (Scheme 1). The reactions were performed at −78 °C, and the products were recrystallized from *n*-hexane and/or CH_2Cl_2 (DCM), respectively. The isolated yields range from 14% (**1**) to 87% (**4a**). The compounds **1**−**5** provide reasonable air stability[21] and good solubility in polar solvents (tetrahydrofuran (THF), CH_2Cl_2) as well as low solubility in most nonpolar solvents (*n*-hexane, toluene, benzene).

Scheme 1. Synthesis of *peri*-Substituted P,Te Systems

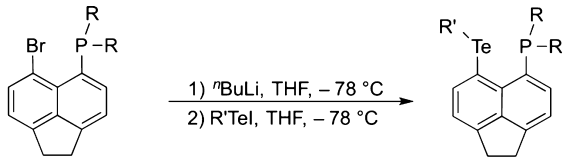

R = ^{i}Pr; R' = Ph (**1**), *p*-An (**2**), Nap (**3**), Mes (**4a**), Tip (**5**)
R = Ph; R' = Mes (**4b**)

1.2. Crystallography. Crystals of compounds **1**−**5** suitable for single-crystal X-ray analysis were isolated after recrystallization from *n*-hexane (**1**, **2**, **3**, **4a**, **5**) and a mixture of *n*-hexane and CH_2Cl_2 (**4b**). The structures are depicted in Figure 3, with important structural parameters shown in Table 1. The phosphorus−tellurium *peri*-distances P···Te1 are in the range of 3.090(1) Å (**2**) and 3.205(2) Å (**4a**) and are thus significantly shorter than the sum of the van der Waals radii ($\sum r_{vdW}$) of phosphorus and tellurium (3.86 Å)[22] (80% of the $\sum r_{vdW}$ for **2**, 83% for **4a**). However, compared to the longest bonds observed for a phosphorus−tellurium bond (2.604(1)[23] or 2.637(3) Å),[24] these distances are significantly longer.

The Te1−C_{Acenap} bond lengths (e.g., 2.146(4) Å for **4a**) are comparable to those of similar compounds (e.g., 2.15(2) Å for *peri*-substituted Br, TePh; 2.16(3)−2.18(2) Å for *peri*-substituted PhTe, TePh)[25] and can thus be seen as a usual Te−C single bond. Likewise the bond length of P−C_{Acenap} (1.821(5) Å for **4a**) is a common length observed for a P−C single bond, especially in similar systems (e.g., 1.846(4) Å for one of the starting materials, the *peri*-substituted Br, P^{i}Pr$_2$).[26,27]

The acenaphthene skeleton of the systems is mainly planar with the central acenaphthene ring torsion angles (e.g., C6−C5−C10−C1 and C4−C5−C10−C9) being close to 180°. As a result of the more attractive interaction the out-of-plane displacements of the phosphorus and tellurium atoms, measured from the mean plane of the acenaphthene, are very small (e.g., 0.176(3) Å for the P atom in **3** and 0.3071(2) Å for the Te atom in **1**). Where most of the X-ray parameters in compounds **1**−**5** are very similar, the Te1−C_{Acenap}−C_{Acenap}−P torsion angle deviates by quite a large range; between −10.7(2)° (**1**) and 10.0(5)° (**3**). Small, negative values for this torsion angle usually indicate that a more attractive interaction exists between the two *peri*-substituted atoms,

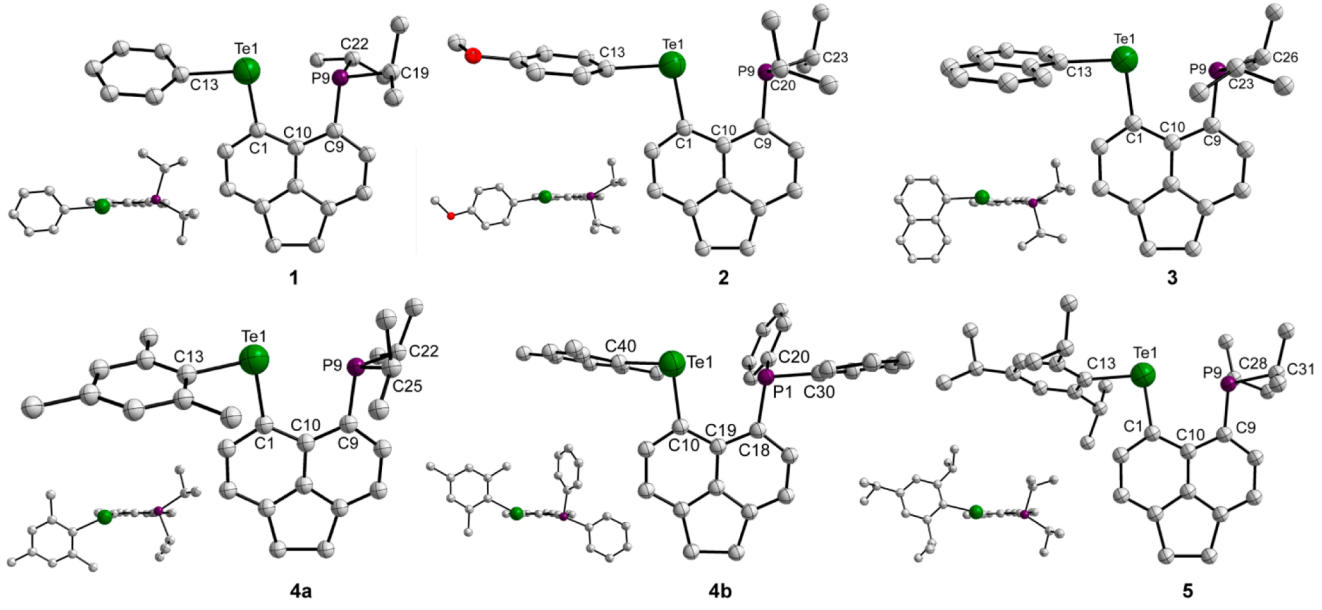

Figure 3. Crystal structures of compounds **1**−**5** (hydrogen atoms and solvent molecules omitted for clarity).

DOI: 10.1021/ic503056z
Inorg. Chem. 2015, 54, 2435−2446

Table 1. Selected Interatomic Distances (Å) and Angles [deg] of the Compounds R′Te−Acenap−PR_2 (R = ^{i}Pr (a), Ph (b)), 1−5

compound	1	2	3	4a	4b	5
peri-moieties (R′)	Ph	MeOPh	Nap	Mes	Mes	Tip
			peri-Region distances and sub-van der Waals contacts			
d(Te1···P)	3.1308(6)	3.090(1)	3.108(2)	3.205(2)	3.181(2)	3.0944(9)
% $\sum r_{vdW}$[a]	81	80	81	83	82	80
			peri-Region bond angles			
Te1−C1−C10 Te1−C10−C19	123.5(2)	124.0(3)	124.2(6)	125.1(3)	125.0(2)	124.6(2)
C1−C10−C9 C10−C19−C18	129.7(2)	129.3(3)	129.5(8)	130.2(4)	129.5(3)	129.0(2)
P−C9−C10 P−C18−C19	120.3(3)	120.1(3)	119.1(7)	119.7(3)	120.9(2)	119.8(2)
$\sum$ of bay angles[b]	373.5(7)	373.4(9)	373(3)	375(1)	375.4(7)	373.4(6)
splay angle	13.5(7)	13.4(9)	13(3)	15(1)	15.4(7)	13.4(6)
			Out-of-plane displacement			
Te1	0.3071(2)	0.0073(3)	0.2731(6)	0.2390(4)	0.0805(3)	0.1487(2)
P	0.1590(6)	0.031(2)	0.176(3)	0.130(2)	0.1130(9)	0.1293(7)
Te1−C1−C9−P Te1−C10−C18−P	−10.7(2)	−0.9(3)	10.0(5)	−7.6(3)	−4.2(2)	6.7(2)
			Central acenaphthene ring torsion angles			
C6−C5−C10−C1 C15−C14−C19−C10	−178.6(3)	179.4(3)	176.3(7)	−176.8(4)	−178.2(4)	178.2(2)
C4−C5−C10−C9 C13−C14−C19−C18	−178.0(3)	−178.5(3)	177.5(7)	−177.6(4)	−178.3(3)	178.7(2)

[a]van der Waals radii used for calculations: r_{vdW}(P) = 1.80 Å; r_{vdW}(Te) = 2.06 Å.[22] [b]Splay angle: $\sum$ of the three bay region angles − 360°. Compounds **1**−**5** show a transoid out-of-plane displacement.

Table 2. Comparison of Bond Lengths and NMR Data of 1−5[a]

compound		*d*(P···Te) [Å] (WBI)	δ ^{31}P NMR [ppm]	δ ^{125}Te NMR [ppm]	*J*(P,$^{125/123}$Te)[33] [Hz]	*J*(P,$C_{ipso\text{-}Aryl}$) [Hz] (WBI)
1	exp	3.131	−20.8	597.4	1306/1084	100
	calc	3.097 (0.18)	−19.5	614	−1185	
2	exp	3.090	−20.4	580.9	1323/1096	100
	calc	3.096 (0.17)	−18.8	582	−1176	
3	exp	3.108	−21.4	483.9	1349/1119	109
	calc	3.088 (0.19)	−19.3	450	−1234	
4a	exp	3.205	−20.9	372.2	1332/1105	93
	calc	3.123 (0.17)	−15.9	307	−1219	88 (0.06)
4b	exp	3.181	−29.5	410.8	1213/1006	74
	calc	3.132 (0.14)	−21.8	383	−1098	74 (0.05)
5	exp	3.094	−21.4	320.9	1357/1127	91
	calc	3.101 (0.17)	−21.8	252	−1200	

[a]Wiberg bond indices (WBI) of the respective interaction given in brackets, NMR chemical shifts and spin−spin coupling constants (for *J*(P,^{125}Te)) for the compounds **1**−**5**.

whereas a larger angle should be observed for a more repulsive interaction. The splay angles for **1**−**5**, defined as the $\sum$ of the three bay region angles −360°,[25] are found to range from 13(3)° (**3**) to 15.4(7)° (**4b**). This value is in accordance with chalcogen−chalcogen or chalcogen−halogen *peri*-substituted acenaphthenes that were reported earlier (16.8° for *peri*-substituted Br−Acenap−TePh; 18.3° for I−Acenap−TePh; 18.4° for PhTe−Acenap−TePh, 15.0° for PhS−Acenap−TePh, 17.1° for PhSe−Acenap−TePh).[25] Larger splay angles mean a more repulsive interaction between the *peri*-substituted atoms, and smaller splay angles indicate a more attractive one.[25]

1.3. NMR Spectroscopy. The NMR parameters of compounds **1**−**5** as well as the calculated values are depicted in Table 2. The calculations of the ^{31}P and ^{125}Te NMR chemical shifts and indirect spin−spin coupling constants confirmed the experimental values within the range of acceptable errors as a result of the calculation process.[28] The ^{31}P NMR spectrum of MesTe−Acenap−P(^{i}Pr)$_2$ (**4a**) consists of a singlet at −20.9 ppm showing satellites for *J*(P,^{125}Te) of 1332 Hz and a set that can be assigned to *J*(P,^{123}Te) of 1105 Hz. Furthermore, small satellites representing *J*(P,C) of 93 Hz can be observed in the ^{31}P NMR spectrum. The ^{125}Te NMR spectrum of **4a** reveals a doublet of doublets at 372.2 ppm showing *J*(^{125}Te,P) of 1337 Hz. For comparison reasons a ^{123}Te NMR spectrum was recorded showing a resonance at 370.2 ppm with a *J*(^{123}Te,P) of 1105 Hz, consistent with the coupling constant observed in the ^{31}P NMR spectrum. The NMR parameters observed in solution and in the solid, ^{31}P and ^{125}Te solid-state NMR spectra of **4a** were recorded (Figure 4).[29] The ^{31}P solid-state magic-angle spinning (MAS) NMR spectrum of **4a** shows a single resonance at −25.8 ppm, with satellites resulting from a coupling to ^{125}Te. The splitting observed in the isotropic peak is 1336 Hz.

Evidence for this spin−spin *J* coupling can also be found in the ^{125}Te solid-state NMR spectrum (acquired using cross-polarization), which exhibits a doublet at 403.1 ppm (note that ^{31}P is 100% abundant). It can be concluded that **4a** does not behave differently within NMR spectroscopic experiments in

DOI: 10.1021/ic503056z
Inorg. Chem. 2015, 54, 2435−2446

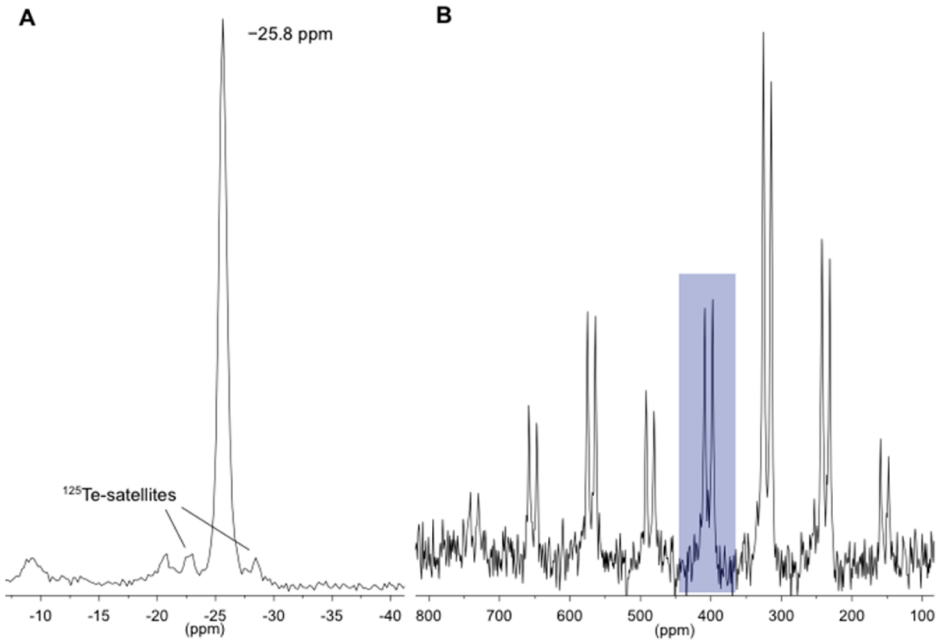

Figure 4. (A) Solid-state ^{31}P NMR spectrum (242.99 MHz, MAS 40 kHz). (B) Solid-state ^{125}Te NMR spectrum (126.28 MHz, 10.5 kHz) of **4a** (the isotropic signal is highlighted).

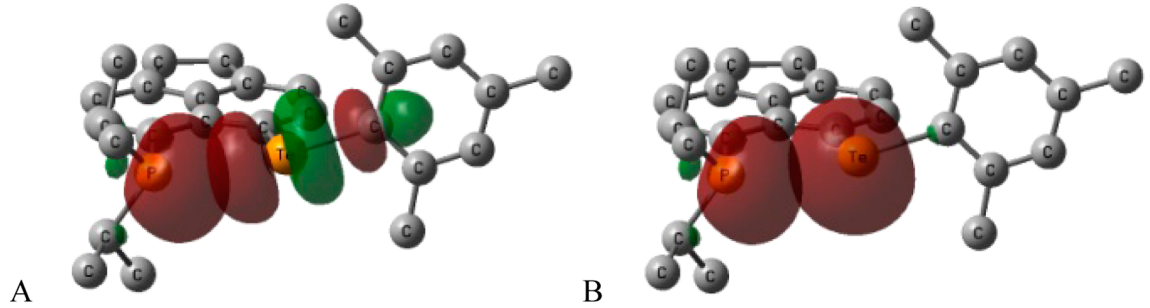

Figure 5. Superposition of selected NBOs of **4a** (B3PW91/SDD/6-311G* level, isovalue 0.04 au)[34] illustrating (A) the lp(P) → σ*(TeC) donor−acceptor interaction and (B) the overlap of the lone pairs on P and Te atoms.

solid state and solution. Compounds **1**−**5** exhibit very similar NMR spectroscopic characteristics to those of **4a** (Table 2). The ^{31}P NMR shifts are in the range from −20.4 (**1**) to −29.5 ppm (**4b**), with J(P,^{125}Te) values ranging from 1213 Hz (**4b**) to 1357 Hz (**5**) and J(P,$C_{ipso\text{-}Aryl}$) values between 74 Hz (**4b**) and 109 Hz (**3**). The differences in the NMR data of systems **1**, **2**, **3**, **4a** and **5**, where different substituents on the tellurium atoms are present, are marginal. In contrast, the deviation of the chemical shift for **4b** is due to the change of the substituents at the phosphorus atom from isopropyl to phenyl. As the P,Te *peri*-distances of **4a** and **4b** are very similar, the explanation for the difference in the J(P,^{125}Te) is presumably due to the different substituent positioning as shown in the solid state structures. A minor overlap of the orbitals involved in the spin transfer explains the different P,Te couplings.[30] The comparison of the P···Te *peri*-distances of **1**−**5** with their P,^{125}Te coupling constants does not allow a direct correlation of the two parameters. Plotting gives an R^2 value of 0.280, which supports the interpretation of an extremely minor correlation with conformation probably being the dominant feature.

Noteworthy are the magnitudes of the J(P,^{125}Te), J(P,^{123}Te), and J(P,$C_{ipso\text{-}Aryl}$) values, especially considering the distance of the phosphorus atoms to the tellurium or carbon atoms. These cannot be explained by through-bond spin−spin coupling constants as couplings through five and six bonds cannot be expected to reach such high values. This phenomenon was first described by Mallory[31] in *peri*-substituted fluorine systems and was recently reviewed by Hierso.[32] The so-called through-space spin−spin coupling is explained by an overlap of lone pair orbitals, which facilitate the transfer of spin information between two atoms.[32] Our recent studies on ditellurides support the conclusion that the major pathway for this transfer is indeed an overlap of lone pair orbitals and not mainly due to a lp(X) → σ*(Y−Z) donor−acceptor interaction.[30] These assumptions were further investigated on a theoretical basis.[33]

1.4. Density Functional Theory Calculations. To give a better explanation of the high values of J(P,^{125}Te), J(P,^{123}Te), and J(P,$C_{ipso\text{-}Aryl}$) and to investigate the nature of the interaction between the phosphorus and the tellurium atom, suitable density functional theory (DFT) calculations were performed. Figure 5 illustrates the superpositions of the natural bonding orbitals (NBO) of MesTe−Acenap−P(^{i}Pr)$_2$ (**4a**) using the B3PW91/SDD/6-311G* level of theory.[34] Figure 5A shows the lp(P) → σ*(Te−C) donor−acceptor interaction that causes the conformations of the ligands that might contribute to the P−Te spin−spin coupling. The calculated energy of this interaction, according to the second-order perturbation analysis, is ∼12 kcal/mol, similar to the lp(Te) → σ*(Te−C)

DOI: 10.1021/ic503056z
Inorg. Chem. 2015, 54, 2435−2446

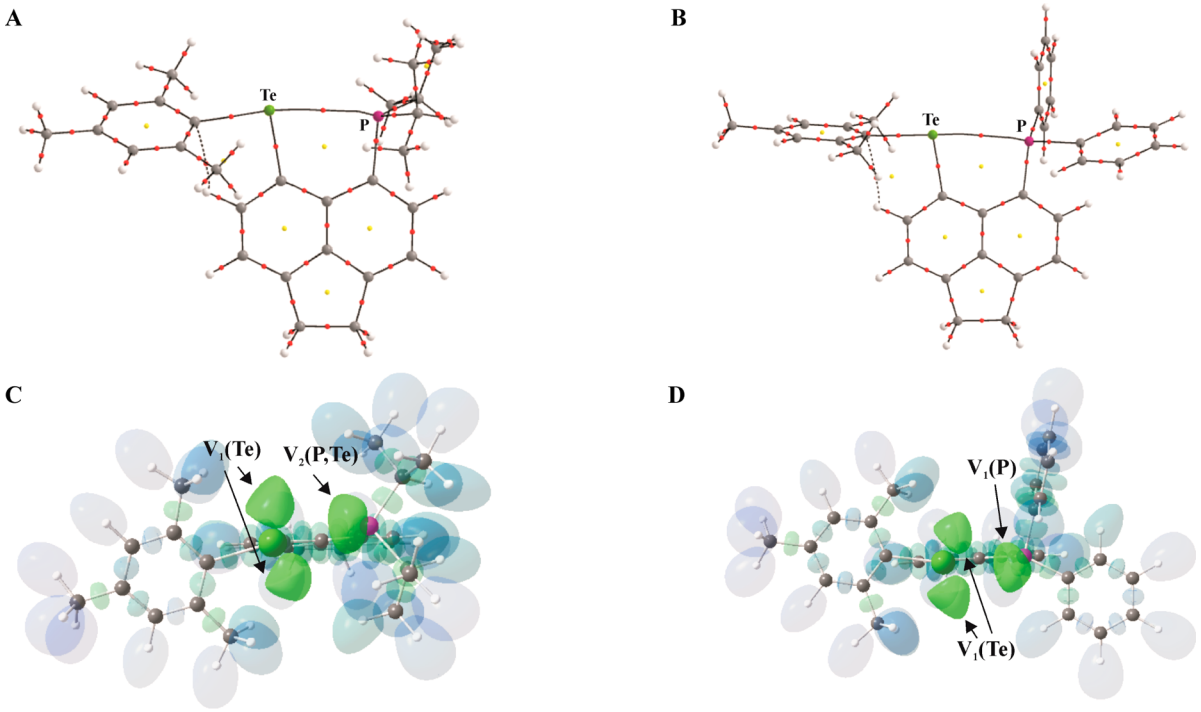

Figure 6. AIM bond paths of **4a** (A) and **4b** (B). Bond critical points are given as red dots, and ring critical points are shown as yellow dots. All structures are AIM2000 representations. Isosurface representation of the localization domains of the ELI-D (Y = 1.40) of **4a** (C) and **4b** (D); the disynaptic basin V_2(Te,P) in **4a** as well as the lone pair basins (V_1) of Te and P are colored green. All remaining ELI-D basins are given in transparent mode for clarity reasons.

Table 3. Calculated Bond Topological and Integrated Bond Descriptors for the Te−P *peri* Interactions of 1−5[a]

	$\rho(r)_{bcp}$ [e·Å^{-3}]	$\nabla^2\rho(r)_{bcp}$ [e·Å^{-5}]	d_1/d [%]	$G/\rho(r)_{bcp}$ [he^{-1}]	$H/\rho(r)_{bcp}$ [he^{-1}]	$N^{ELI}_{(001)}$ [e]	$V^{ELI}_{(001)}$ [Å^3]	Y_{max}	Δ_{ELI} [Å]	RJI [%]
1	0.19	1.0	51.2	0.46	−0.10	2.06	12.45	2.27	0.50	97.5
2	0.19	1.0	50.9	0.46	−0.10	2.07	12.74	2.30	0.59	98
3	0.20	1.0	51.4	0.46	−0.10	2.06	12.33	2.26	0.49	97
4a	0.18	1.0	51.0	0.47	−0.09	2.08	12.88	2.30	0.56	98
4b	0.17	1.0	50.4	0.47	−0.08	2.03	13.16	2.35		97.9
5	0.19	1.0	50.9	0.46	−0.10	2.07	12.69	2.30	0.59	98

[a]For all bonds, $\rho(r)_{bcp}$ is the electron density at the bond critical point, $\nabla^2\rho(r)_{bcp}$ is the corresponding Laplacian, d_1 is the distance from the atom to the bond critical point, $G/\rho(r)_{bcp}$ and $H/\rho(r)_{bcp}$ are the ratios of kinetic and total energy over $\rho(r)_{bcp}$. For all basins, $V^{ELI}_{(001)}$ is the basin volume cut at 0.001 au, $N^{ELI}_{(001)}$ is the corresponding electron population in that volume, Y_{max} is the ELI-D value at the attractor position, Δ_{ELI} is the perpendicular distance of the attractor position to the atom−atom line, and RJI is the Raub−Jansen index (percentile electron population within the AIM atom that has the larger electronegativity).

donor−acceptor interaction found in *peri*-substituted ditellurides. High values of the Wiberg bond index (WBI)[35] of compounds **1**−**5** are of particular interest, as these are in the range from 0.14 to 0.19. Whereas single bonds usually approach values of 1, the figures for a significant three-center four-electron bond (3c−4e) were reported to be ∼0.55 (for 1,6-dibromo-2-phenyl-1,2-diselenaacenaphthylene with d(Se−Se) = 2.516 and 2.542 Å).[15,36] However, weak three-center four-electron type interactions were discussed for compounds with a WBI of ∼0.14 to 0.19 (e.g., PhTe−Acenap−TePh, radical cations of PhSe−Nap−P(E)Ph$_2$ (E = O, S, Se)).[15,25] The mesomeric Lewis structures that result from this interpretation can be written as [R$_3$P| Te−C ⇔ R$_3$P$^+$−Te |C$^-$] involving four electrons on three centers. As a result, the interaction between the phosphorus and the tellurium atom as well as the carbon atom of the ligand ($C_{ipso\text{-}aryl}$) bonded to the tellurium can be described as an "onset" three-center (P, Te, $C_{ipso\text{-}aryl}$) four-electron type interaction. The large through-space couplings of J(P,^{125}Te) of 1332 Hz and through-space and one bond J(P,$C_{ipso\text{-}Aryl}$) of 93 Hz support the interpretation that significant interaction between the atoms must be present. However, the lp(Te) → σ^*(Te−C) donor−acceptor interaction alone cannot explain the large values of the spin−spin coupling constants, as the expected values would be much smaller. Additional interaction must be involved to satisfy spin−spin couplings between the phosphorus and tellurium atom. Figure 5B illustrates the overlap of the lone pairs on the phosphorus and the tellurium atom that might be responsible for the transfer of spin information between both nuclei and the resulting observation of large P,Te coupling constants. [It is the s-type lone pair on Te (80% s character for the NBO shown in Figure 5B) that is key for transmission of the spin−spin coupling, rather than the essentially pure p-type lone pair orbital] This expectation is derived from our calculations of the Te−Te coupling pathway of the ditelluride MeTe−Nap−TePh, where a visualization of this coupling path shows the largest contribution from regions where such lone pairs would overlap, and smaller contributions from the Te−C bonds involved in

DOI: 10.1021/ic503056z
Inorg. Chem. 2015, 54, 2435−2446

the donor−acceptor interaction.[30] In the systems **1**−**5** the donor−acceptor interaction could lock the system in a conformation where the overlap of the lone pairs leads to the high couplings observed. Thus, it is expected that this interaction is just as important, if not more important, for the large coupling constants as the lp(Te) → σ^*(Te−C) donor−acceptor interaction. Consistent with this interpretation, the calculated (Te,P) couplings (ZORA-Spinorbit/BP86 level) are clearly dominated by the Fermi-contact (and spin-dipolar) terms. The observed difference of ∼20 Hz in the $J(P,C_{ipso\text{-}Aryl})$ coupling of **4a** and **4b** was supported by the calculated values of the NBO analyses of the different lp(P) → σ^*(Te−C) (88 and 74 Hz, respectively). The WBI of the P···$C_{ipso\text{-}Aryl}$ interaction was calculated to be 0.06 for **4a** (11.7 kcal/mol) and 0.05 (10.4 kcal/mol) for **4b**. Consistently the WBI for the Te−$C_{ipso\text{-}aryl}$ bond is slightly larger in **4b** (0.84; 0.82 for **4a**). A complementary analysis of a set of topological and integrated real-space bonding indicators (RSBI) derived from the electron and electron-pair densities according to the atoms in molecules (AIM)[37] and electron localizability indicator (ELI-D)[38] allows a further insight into the nature of the P···Te *peri*-interaction. The topological bond path motifs as well as an isosurface representation of the ELI-D of **4a** and **4b** are displayed in Figure 6 (corresponding data of **1**−**3** and **5** are shown in the Supporting Information). Table 3 presents bond topological properties derived from AIM space partitioning and a set of ELI-D derived properties of **1**−**5**. In all compounds **1**−**5**, a P···Te bond critical point (bcp) is found and shows the characteristics of mainly ionically bonded atoms, indicated by small values of the electron density at the bcp (0.17 eÅ^{-3} (**4b**) to 0.20 eÅ^{-3} (**3**)), a positive but close to zero Laplacian, a positive kinetic energy to $\rho(r)_{bcp}$ ratio, and a negative but close to zero total energy to $\rho(r)_{bcp}$ ratio. The relative position of the bcp varies marginally from 50.9% in **4b** to 51.4% in **3**. In general the ELI-D confirms the AIM results. In **4b** a monosynaptic V_1(P) basin is found, which represents the lone pair at the phosphorus atom; all other compounds show a disynaptic V_2(P,Te) basin, but the assignment of the disynaptic basins in **1**−**4a** and **5** can be stated to be in a border regime to a lone pair basin as the V_2(P,Te)/V_1(P) basins are located much closer to the phosphorus than to the tellurium atom, which means that the P···Te *peri*-interaction is mainly established by the phosphorus (see Figure 6). As expected, the Raub Janzen index (RJI)[39] shows values in the range of 97% (**3**) to 98% (**2**, **4a**, **5**), which means that 97% (in **3**) of the electron density of the V_2(P,Te) basin remains in the AIM atomic basin of the phosphorus atom and is consistent with a weakly coordinative to an almost nonbonding scenario. It is worth noting that the different substituents bound to the tellurium and phosphorus have only small effects on the V_2(P,Te)/V_1(P) basin electron populations (2.03 e (**4b**) to 2.08 e (**4a**)) and volumes (12.45 Å^3 (**1**) to 13−16 Å^3 (**4b**)). In contrast to the NBO picture of the lone pairs P and Te atoms pointing at each other (Figure 5B), the ELI-D results more closely resemble the classic Lewis picture of a steric interaction between the P atom lone pair, which forms a coordinative bond to the positively charged Te core, and two Te atom lone pairs being part of an almost tetrahedral coordination sphere around the Te atom together with the two Te−C bonds. The Te atom lone pairs are restrained between the P atom lone pair on the one side and the protonated monosynaptic valence basins ("H atoms") of the mesityl-fragment methyl groups on the other side, which is reflected in the flattening of all three types of basins, see Figure 6C,D.

2. INFLUENCE OF THE PHOSPHORUS OXIDATION AND COMPLEXATION OF THE SYSTEMS 4A AND 4B

2.1. Synthesis. The oxidation of the derivatives of **4** using elemental sulfur or selenium in refluxing toluene or THF, respectively, yielded the P^V systems **6** and **7** (Scheme 2). Metal complexes were obtained by the facile reaction of **4a** with (COD)$PtCl_2$ or AuCl·THT (THT = tetrahydrothiophene) in CH_2Cl_2 at room temperature (Scheme 2).

Scheme 2. Reactions of *peri*-Substituted P,Te Systems

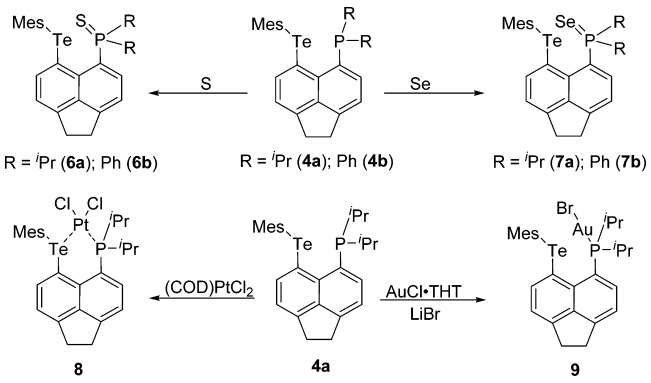

Compounds **6**−**7** were obtained in yields of 52% (**7b**) to 91% (**6a**), but **8** can be isolated almost quantitatively. Compound **9** was obtained as a minor product (16%) as part of a complicated reaction mixture as observed by ^{31}P NMR spectroscopy.

2.2. Crystallography. Crystals of compounds **6**−**9** suitable for single-crystal X-ray analysis were isolated after recrystallization from *n*-hexane (**6a** and **7a**), a mixture of *n*-hexane and CH_2Cl_2 (**6b** and **7b**), or pure CH_2Cl_2 (**8** and **9**). Illustrations of the structures **6**−**9** are shown in Figure 7, and structural parameters are depicted in Table 4. The oxidation of the phosphorus atoms in **4a** and **4b** to yield MesTe−Acenap−P(E)(^{i}Pr)$_2$ (E = S (**6a**); Se (**7a**)) and MesTe−Acenap−P(E)Ph_2 (E = S (**6b**); Se (**7b**)) causes the formation of a much more sterically demanding system when compared to its P^{III} derivatives. The P···Te *peri*-distance in **6a**, for example, elongates to 3.6190(6) Å (cf. 3.205(2) Å in **4a**) but is still shorter than the sum of the van der Waals radii (3.86 Å).[22] The splay angles extend to the range of 22.7(7)° (**6a**) and to 26(2)° (**7b**) (cf. 15(1)° in **4a**), so that the species **6** and **7** can be interpreted as stronger repulsive systems when compared to **4a** and **4b**. Consistently, the out-of-plane displacement of the tellurium atom increases to higher values (e.g., 0.70(2) Å (**6a**), 0.51(4) Å (**6b**), cf. 0.23(4) Å for **4a**, 0.08(3) Å for **4b**) and for the phosphorus atom to smaller values (0.61(6) Å for **6a**, 0.35(2) Å for **6b**; cf. 0.13(2) Å for **4a**, 0.11(9) Å for **4b**), which causes the Te−C−C−P torsion angle to increase as well (30.7(2)° for **6a**, −7.6(3)° for **4a**). The central acenaphthene ring torsion angles decrease (in **6a** to 171.3(3)° and 174.8(3)°), which then deviate more significantly from the ideal 180° angle when compared to the starting material **4** (e.g., −176.8(4)° and −177.6(4)° for **4a**). The Te···S distance in **6a** (3.1511(7) Å) and **6b** (3.183(2) Å) are significantly smaller than the sum of van der Waals radii of tellurium and sulfur

DOI: 10.1021/ic503056z
Inorg. Chem. 2015, 54, 2435−2446

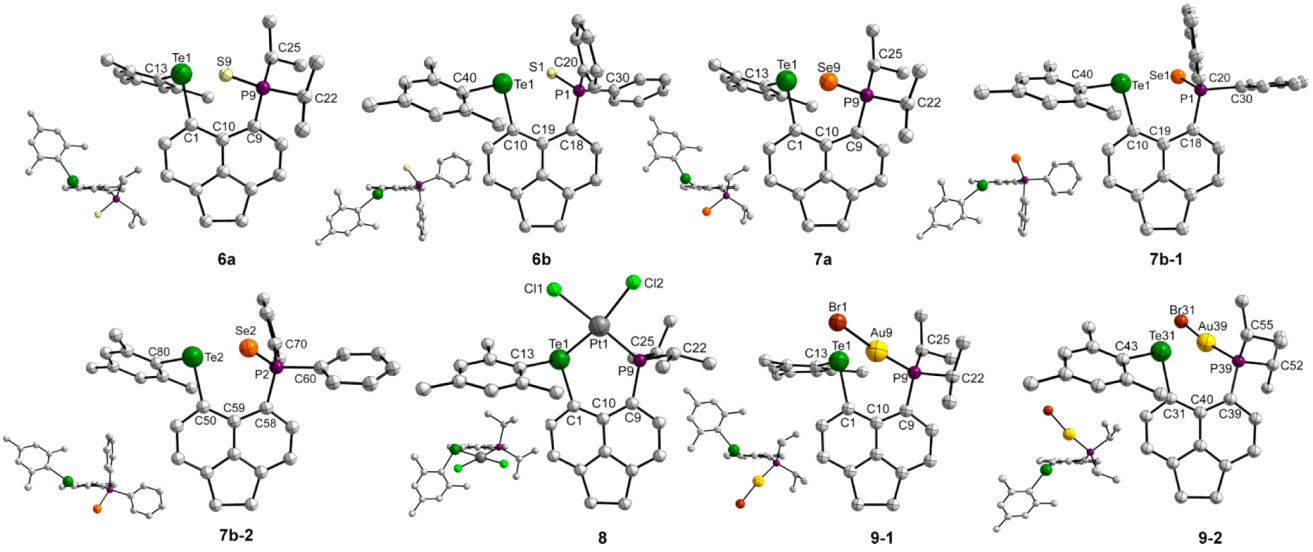

Figure 7. Crystal structures of compounds **6**–**9** (hydrogen atoms and solvent molecules omitted for clarity).

Table 4. Selected Interatomic Distances (Å) and Angles [deg] of the Compounds R′Te−Acenap−PR (R = ^{i}Pr (a), Ph (b)), 6–9

compound	**6a**	**6b**	**7a**	**7b**	**8**	**9**
X =	S	S	Se	Se	Pt	Au
d(Te1−X)					2.4801(4)	
d(P−X)	1.9652(8)	1.951(2)	2.1211(7)	2.108(2) [2.107(2)]	2.2430(8)	2.259(5) [2.251(5)]
peri-region distances and sub-van der Waals contacts						
d(Te1···P)	3.6190(6)	3.554(2)	3.6426(7)	3.573(3) [3.580(3)]	3.5081(7)	3.555(5) [3.548(6)]
% $\sum r_{vdW}$[a] (Te1···P)	94	92	94	93 [93]	91	92 [92]
d(Te1···X)	3.1511(7)	3.183(2)	3.2515(4)	3.419(2) [3.305(2)]		3.128(2) [3.141(2)]
peri-region bond angles						
Te1−C1−C10 Te1−C10−C19	126.2(2)	127.1(2)	126.5(2)	128.0(3) [127.3(3)]	126.9(2)	128(2) [125(2)]
C1−C10−C9 C10−C19−C18	130.7(3)	130.9(3)	130.4(2)	131.2(4) [131.0(4)]	130.7(2)	130(2) [130(2)]
P−C9−C10 P−C18−C19	125.8(2)	125.7(2)	125.9(2)	126.5(3) [126.1(3)]	128.6(2)	126(2) [125(2)]
$\sum$ of bay angles[b]	382.7(7)	383.7(7)	382.8(6)	386(2) [384(2)]	386.2(6)	384(6) [380(6)]
splay angle	22.7(7)	23.7(7)	22.8(6)	26(2) [24(2)]	26.2(6)	24(6) [20(6)]
Out-of-plane displacement						
Te1	0.7099(2)	0.5132(4)	0.7070(2)	0.3415(4) [−0.5493(4)]	0.1127(4)	0.485(2) [0.655(2)]
P	0.6161(6)	0.350(2)	0.6552(6)	−0.153(2) [0.320(2)]	0.0722(7)	0.530(4) [0.675(6)]
X	1.7184(6)	1.640(2)	1.9061(3)	−1.8056(6) [1.7713(5)]	0.6606(4)	1.8908(6) [1.9160(6)]
Te1−C1−C9−P Te1−C10−C18−P	30.7(2)	−19.8(3)	31.6(2)	−13.0(4) [19.7(3)]	−5.1(2)	24.3(9) [−32(1)]
Central acenaphthene ring torsion angles						
C6−C5−C10−C1	171.3(3)	−175.3(4)	171.2(3)	179.8(6) [175.0(5)]	−179.8(2)	178(2) [−176(2)]
C15−C14−C19−C10						
C4−C5−C10−C9	174.8(3)	−176.8(4)	174.6(3)	−179.0(5) [176.6(6)]	−178.4(2)	171(2) [−172(2)]
C13−C14−C19−C18						

[a]van der Waals radii used for calculations: r_{vdW}(P) = 1.80 Å; r_{vdW}(Te) = 2.06 Å.[22] [b]Splay angle: $\sum$ of the three bay region angles − 360·. Compounds **6**–**9** show a transoid out-of-plane displacement.

(3.86 Å).[22] As a result an orbital interaction between these atoms can be expected similar to the one discussed for the P,Te interaction in **1**–**5**. The sulfur in **6a** and **6b** is bonded over a P═S double bond (1.9652(8) Å (**6a**); 1.9514(15) Å (**6b**)) and deviates 1.7184(6) Å (**6a**) or 1.640(2) Å (**6b**) from the mean plane of the acenaphthene backbone. The selenium derivatives **7a** and **7b** are mainly isostructural with their sulfur derivatives **6a** and **6b**, including similar values describing the out-of-plane displacement as well as the central acenaphthene ring torsion angles (cf. Table 4). The Se···Te distance of 3.2515(4) Å (**7a**) and 3.419(2)/3.305(2) Å (**7b**) are significantly smaller than the sum of the van der Waals radii of a tellurium and a selenium atom (3.96 Å). As proposed for **6** this could result in a significant interaction of the two atoms as discussed in the NMR Spectroscopy and DFT Calculations sections.

[MesTe−Acenap−P(^{i}Pr)$_2$][μ-PtCl$_2$] (**8**) exhibits a bridging Pt atom that connects the *peri*-substituted phosphorus and tellurium atoms that are bonded to the acenaphthene ring. The ligands at the platinum atom adopt a distorted planar environment. The P···Te *peri*-distance of 3.5081(7) Å (cf. 3.205(2) Å for **4a**) is shorter than the sum of the van der Waals radii (3.86 Å),[22] as observed for all aforementioned examples (**1**–**7**).

The splay angle of 26.2(6)° in **8** is slightly enhanced, when compared to those of the sulfur (**6a**, 22.7(7)°) and selenium (**7a**, 22.8(6)°) derivatives, suggesting a more repulsive system.

DOI: 10.1021/ic503056z
Inorg. Chem. 2015, 54, 2435−2446

In contrast, the out-of-plane displacement is minor, with the tellurium atom deviating 0.1127(4) Å and the phosphorus atom 0.0722(7) Å from the mean plane of the acenaphthene backbone. The distance of the Pt atom to the mean plane is 0.6606(4) Å. The central acenaphthene torsion angles of **8** are both close to 180° (cf. −179.8(2)° and −178.4(2)°), which suggests a rather relaxed geometry of the acenaphthene backbone.

Two independent molecules of [MesTe−Acenap−P(^{i}Pr)$_2$]-[AuBr] (**9**) were found within the crystal structure exhibiting different positions for the Mes ligand and the AuBr moiety. In contrast to the platinum complex **8** the gold atom in **9** is coordinated to the phosphorus atom only. However, the P−Au−Br angles are 173.6(2)° and 171.2(2)° (Br31−Au39−P39), respectively, where the Au atom is bent toward the Te atom indicating an interaction through space. The observed Au···Te distance is 3.128(2) Å [3.141(2) Å for the second molecule], whereas Au−Te bonds are reported with bond lengths of ∼2.6 Å (e.g., 2.6149(8)−2.6446(9) Å in the Au(III) complex [{Ph$_2$PNP(Te)Ph$_2$}Au(μ-Te)]$_2$[40] and 2.616(7)−2.639(1) in the Au(I) complex Au(PPh$_3$)[N(^{i}Pr$_2$PTe)$_2$][41]). The interaction in **9** is indicative of a fractional (partial) Au···Te bond (cf. the notable WBI of 0.16 between both atoms, Table 5).

The *peri*-distances between the phosphorus and tellurium atoms are 3.555(5) and 3.548(6) Å, respectively, which is ∼92% of the sum of van der Waals radii (cf. 3.86 Å).[22] The central acenaphthene torsion angles of 178(2)° [−176(2)°] and 171(2)° [−172(2)°] indicate a constrained system toward the phosphorus atom. The tellurium atom deviates 0.48(2) Å [0.65(2) Å] and the phosphorus atom 0.53(4) Å [0.67(6) Å] from the mean plane of the acenaphthene. The distance of the Au atom from this plane is 1.89(6) Å [1.91(6) Å for the second molecule].

2.3. NMR Spectroscopy. The NMR parameters of the compounds **6**−**9**, as well as the calculated values, are summarized in Table 5. As expected the oxidation of the phosphorus atoms in **4** to give **6** and **7** has a significant influence on the P,Te through-space spin−spin coupling, as the lone pair at the phosphorus atom is no longer available for the transfer of spin information. This was also observed in the *peri*-substituted phosphorus−selenium systems Ph$_2$(E)P−Nap−SePh (E = O, S, Se)).[15,32]

The ^{31}P NMR spectrum of MesTe−Acenap−P(S)(^{i}Pr)$_2$ (**6a**) depicts a single resonance at 62.2 ppm (cf. 46.5 ppm for **6b**) with no visible P−Te couplings for both sulfur compounds. The oxidation of the P^{III} atom to the P^V species causes a decrease in the shielding and a subsequent downfield shift when compared to **4a** or **4b** (−20.9 ppm, −29.5 ppm). However, calculations suggest a small P−Te coupling of 15 Hz for **6a**, which could be hidden under the phosphorus resonance in the experimental spectrum. The coupling could either be a result of a ^4J(P,Te) or, more likely, a partial through-space coupling (P═S···Te). The ^{125}Te NMR spectrum of **6a** exhibits a broad singlet at 447.0 ppm, the one of **6b** a singlet at 488.1 ppm.

The ^{31}P NMR of MesTe−Acenap−P(Se)(^{i}Pr)$_2$ (**7a**) exhibits a singlet at 55.6 ppm and that of the MesTe−Acenap−P(Se)Ph$_2$ (**7b**) a singlet at 35.0 ppm. These signals are accompanied by ^{125}Te satellites that reveal small P−Te couplings of 13 Hz (**7a**) and 21 Hz (**7b**), respectively, as well as ^{77}Se satellites, which show a ^1J(P,Se) of 695 Hz (**7a**) and 697 Hz (**7b**). The ^{77}Se NMR spectrum features a doublet at −353.7 ppm (**7a**, −177.8 ppm for **7b**), whereas the ^{125}Te NMR consists of a doublet at 448.5 ppm (**7a**) or at 492.8 ppm (**7b**). The resonances are accompanied by ^{77}Se satellites revealing a J(^{125}Te,^{77}Se) of 684 Hz (**7a**) and 566 Hz (**7b**). The calculated value of −510 Hz (**7a**; −411 Hz for **7b**) for this interaction is slightly smaller. Such a large coupling constant can be explained by the interaction of two nonbonding orbitals of the two chalcogen atoms that transfer the spin information through space (cf. Ph$_2$(Se)P−Nap−SePh).[15,32] Furthermore, the J(Te,Se) coupling in **7** is much smaller in magnitude than the J(Te,P) in **1**−**5**, which is largely due to the gyromagnetic ratios—in terms of reduced coupling constants, both would be much more similar as the K(Te,Se) is ca. 10% smaller than the K(Te,P). The ^{31}P NMR spectrum of [MesTe−Acenap−P(^{i}Pr)$_2$][μ-PtCl$_2$] (**8**) consists of a singlet at 14.5 ppm accompanied by ^{195}Pt satellites revealing a ^1J(P,^{195}Pt) of 3482 Hz. The ^{125}Te NMR spectrum exhibits a doublet at 472.9 ppm (J(P,^{125}Te) = 17 Hz) with a ^1J(^{125}Te,Pt) value of 695 Hz. Furthermore, a doublet at −4412 ppm is observed in the ^{195}Pt NMR spectrum confirming the ^1J(P,^{195}Pt) observed in the ^{31}P NMR spectrum. The ^{31}P NMR spectrum of [MesTe−Acenap−P(^{i}Pr)$_2$][AuBr] (**9**) exhibits a single resonance at 46.8 ppm. The singlet is accompanied by ^{125}Te satellites revealing a J(P,Te) value of 292 Hz. This coupling constant might be too large to be a result of a spin transfer through bonds. Similar to the aforementioned [X$_2$M][Fc(PPh$_2$)$_4$^{t}Bu$_2$] species[32,42] the overlap of a lone pair orbital at the tellurium atom with an electron pair shared by the phosphorus and gold atom may cause the transfer of spin information. The ^{125}Te NMR consists of a doublet at 470.1 ppm, which confirms the J(P,Te) value observed in the phosphorus NMR spectrum.

2.4. Density Functional Theory Calculations. The systems **6**−**9** were also investigated by suitable DFT calculations. In contrast to compounds **1**−**5**, the P−Te WBI values of 0.02 to 0.06 found in compounds **6** to **9** indicate a very minor interaction between the nonbonded P and Te atoms in these compounds. Apart from compound **9**, this is in agreement with the very small coupling constants found in these systems (Table 5).

Compared to the Te···P interaction in **1**−**5**, the Te···Se interaction in **7a** and **7b** seems to be slightly weaker, as the WBI is only 0.11 and 0.10, respectively. The NBO analysis localizes three lone pairs on the Se atoms (corresponding to the polar R3P$^+$−Se$^-$ formulation, where one of them is involved in a donor−acceptor interaction with the σ*(Te−C$_{ipso\text{-}aryl}$) bond (7.6 kcal/mol for **7a** in the second-order perturbation analysis). The NMR analyses of **7a** and **7b** show large Te−Se coupling constants of 684 and 566 Hz, respectively, which support the assumption of an orbital interaction between the Te and Se atoms. Similar interactions were calculated for the compounds **6a** and **6b**, where a weak Te···S interaction is involved (WBIs of 0.10 and 0.09). As sulfur is not NMR active these are not observable experimentally.

The Au···Te interaction in **9** seems quite notable with a WBI of 0.16 (compared to 0.72 and 0.63 for Au−Br and Au−P, respectively). The NBO analysis finds localized Au−Br and Au−P bonds and five lone pairs on Au (the d-orbitals). However, the back-donation from these d-orbitals into the σ*(Te−C) orbital (similar to the donor−acceptor interactions discussed above) seems very weak (3 kcal/mol). The (Te,P) coupling of 292 Hz (calculated to be −221 Hz) in **9** is quite large, considering that it would be transferred over a full (Au−P) and a more partial bond (Au···Te). Although in the NBO analysis of compound **9** a localized Au−P bond is found, the

DOI: 10.1021/ic503056z
Inorg. Chem. 2015, 54, 2435−2446

Table 5. Comparison of Bond Lengths and NMR Data of 6–9[a]

compound	d(P···Te) [Å] d(P··· Te) [Å] (WBI) (calc1) d(Te··· X) [Å] (WBI) (calc2)	δ ^{31}P NMR [ppm]	δ ^{125}Te NMR [ppm]	J(P,^{125}Te) [Hz]	δ_x [ppm] (J(P···X)) [Hz]	J [Hz]
6a	exp 3.619	exp 62.2	exp 447.0	-	-	-
	calc1 3.640 (0.02)	calc 63.2	calc 405	calc 15		
	calc2 3.201 (0.10)					
6b	exp 3.554 (2)	exp 46.5	exp 488.1	-		
	calc1 3.561 (0.03)	calc 46.9	calc 459	calc −1		
	calc2 3.243 (0.09)					
7a	exp 3.643	exp 55.6	exp 448.5	exp 13	exp ^{77}Se = −353.7 (695)	exp Te−Se = 684
	calc1 3.363 (0.03)	calc 62.3	calc 399	calc 13	calc ^{77}Se = −286	calc Te−Se = −510
	calc2 3.286 (0.11)					
7b	exp 3.573(3) [3.580(3)]	exp 35.0	exp 492.8	exp 21	exp ^{77}Se = −177.8 (697)	exp Te−Se = 566
	calc1 3.580 (0.03)	calc 33.3	calc 468	calc −12	calc ^{77}Se = −106	calc Te−Se = −411
	calc2 3.332 (0.10)					
8	exp 3.508	exp 14.5	exp 472.9	exp 17	exp ^{195}Pt = −4412	exp Te−Pt = 695
	calc1 3.561 (0.06)	calc 7.9	calc 471	calc −1	calc ^{195}Pt = −1874[43]	calc Te−Pt = 1578
	calc2 2.543 (0.75)					
9	exp 3.555	exp 46.8	exp 470.1	exp 292		
	calc1 3.552 (0.04)	calc 32.1	calc 379	calc −221		
	calc2 3.203 (0.16)					

[a]First line: Experimental values. Second and third lines: Computed bond distances, with Wiberg bond indices (WBI) of the respective interaction given in brackets, and NMR chemical shifts and spin−spin coupling constants for the compounds **6–9**.

DOI: 10.1021/ic503056z
Inorg. Chem. 2015, 54, 2435−2446

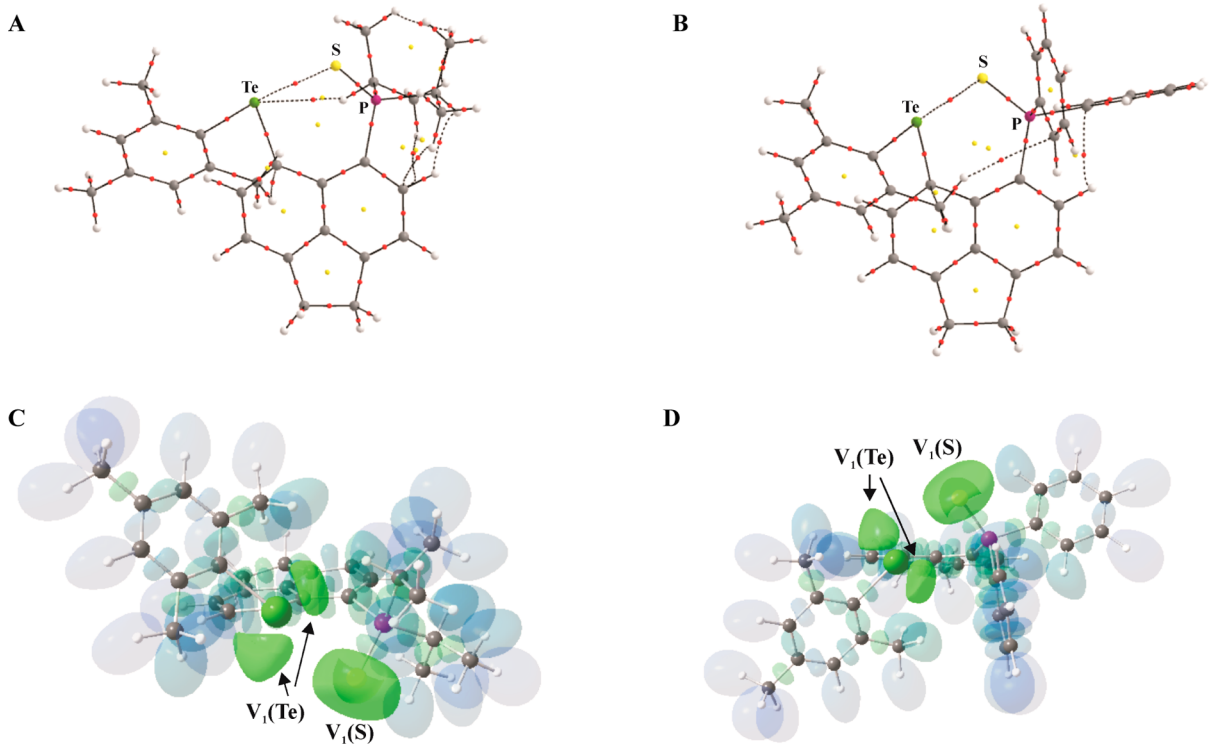

Figure 8. AIM bond paths of **6a** (A) and **6b** (B). Bond critical points are given as red dots, and ring critical points are shown as yellow dots. All structures are AIMAU representations. Isosurface representation of the localization domains of the ELI-D ($Y = 1.40$) of **6a** (C) and **6b** (D); the lone pair basins (V_1) of Te and S are colored green. All remaining ELI-D basins are given in transparent mode for clarity reasons.

Table 6. Calculated Bond Topological and Integrated Bond Descriptors for the Te−E Interactions of 6−9 (E = S, Se, Pt, Au)[a]

	X···Te	$\rho(r)_{bcp}$ [e·Å^{-3}]	$\nabla^2\rho(r)_{bcp}$ [e·Å^{-5}]	d_1/d [%]	$G/\rho(r)_{bcp}$ [he^{-1}]	$H/\rho(r)_{bcp}$ [he^{-1}]
6a	S···Te	0.15	1.0	50.5	0.53	−0.04
6b	S···Te	0.14	1.0	50.6	0.52	−0.03
7a	Se···Te	0.15	0.9	51.4	0.49	−0.04
7b	Se···Te	0.14	0.9	51.4	0.49	−0.03
8	Pt···Te	0.61	1.5	51.1	0.57	−0.40
9	Au···Te	0.16	1.2	50.4	0.57	−0.06

[a]For all bonds, $\rho(r)_{bcp}$ is the electron density at the bond critical point, $\nabla^2\rho(r)_{bcp}$ is the corresponding Laplacian, d_1 is the distance from the atom to the bond critical point, and $G/\rho(r)_{bcp}$ and $H/\rho(r)_{bcp}$ are the ratios of kinetic and total energy over $\rho(r)_{bcp}$.

latter is heavily polarized toward P (80% P character, essentially pure sp^3 on P), thus retaining much "lone pair" character. In contrast, the P−X bond in the P═X compounds (X = S, Se) is more evenly shared between P and X; thus, it has a much smaller overall contribution from P, ca. 50%. (Only one P−X bond is labeled as such; the other is localized as additional lone pair on X.) Together with the slightly shorter Te···P distance in the Au complex (3.55 vs >3.6 Å in **6** and **7**, Table 5), this can rationalize the sizable coupling observed in **9** (see Figure S4 in the Supporting Information for a visualization of this different extent of overlap). In the calculation the Te,P coupling is significantly larger than the Te,P couplings in the P═S or P═Se systems **6** and **7**, even if the WBI of the Te,P interaction in **9** was calculated to be 0.04 and thus as small as that for systems **6** and **7**. This prompted us to expect that other interactions between the Te and Au atoms are involved that help transmit that coupling. An explanation could be found by Hierso et al., who showed that also only one lone pair orbital, which interacts with a bonding orbital, can transfer nuclear spin information through space.[42] The possible pathway of the spin information transfer in **9** would thus be through a lone pair orbital of the Te atom to the bonding Au−P orbital. This could explain the high Te,P coupling constant. The topological bond path motifs of **6a** and **6b**, as well as an isosurface representation of the ELI-D, are displayed in Figure 8 (corresponding topological bond paths motifs of **7**−**9** are shown in the Supporting Information). Table 6 presents bond topological properties derived from AIM space partitioning and a set of ELI-D derived properties of **6**−**9**. As expected no P···Te bcp were found in compounds **6**−**9**; instead, X···Te bcp were detected. In case of the sulfur (**6a** and **6b**), selenium (**7a** and **7b**), and gold (**9**) compounds small electron densities at the bcp (0.14 eÅ^{-3} (**6b** and **7b**) to 0.16 eÅ^{-3} (**9**)), a positive but close to zero Laplacian, a positive $G/\rho(r)_{bcp}$ ratio, and a negative but close to zero $H/\rho(r)_{bcp}$ ratio was found and indicate a mainly ionic X···Te bonding situation. In comparison the Pt···Te interaction in **8** shows a higher electron density at the bcp of 0.61 e and an $H/\rho(r)_{bcp}$ ratio of −0.40 he^{-1} indicating a polar covalent bonding situation.

CONCLUSIONS

The *peri*-substituted phosphorus−tellurium systems R′Te−Acenap−PR$_2$ (R′ = Ph, *p*-An, Nap, Mes, Tip; R = ^{i}Pr, Ph) are

DOI: 10.1021/ic503056z
Inorg. Chem. 2015, 54, 2435−2446

readily available by the addition of organotellurium monohalides to lithiated R_2P–Acenap–Li systems. The resulting species exhibit large "through-space" spin–spin coupling constants and interactions that can be described as the "onset" of three-center four-electron type interactions. Oxidation of the phosphorus atoms by sulfur and selenium resulted in a disappearance of the strong P–Te coupling as lone pair orbitals are no longer available for the interaction with those of the tellurium atom. Complexation resulted in a similar observation in the case of platinum, whereas a gold complex was shown to exhibit relatively large P–Te couplings that are presumably a result of an overlap of a tellurium lone pair orbital with a P–Au bonding orbital. Figure 9 illustrates the three

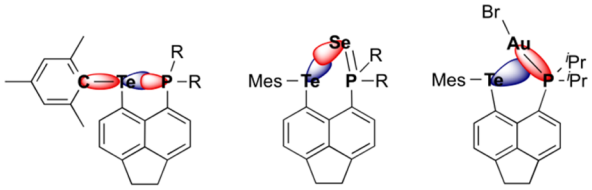

Figure 9. Proposed orbital interactions in the compounds **4**, **7**, and **9** causing the transfer of spin information through space.

different pathways of the transfer of spin information through space that were discussed in this work. Additionally to the overlapping lone pair orbitals, a certain contribution of donor–acceptor interactions might be responsible for the observed coupling constants, whereas the through-bond coupling is expected to contribute to a very minor degree.

■ ASSOCIATED CONTENT

Supporting Information

Experimental and crystallographic data of the new compounds as well as computational details. This material is available free of charge via the Internet at http://pubs.acs.org.

■ AUTHOR INFORMATION

Corresponding Authors

*E-mail: j.beckmann@uni-bremen.de. (J.B.)
*E-mail: jdw3@st-andrews.ac.uk. (J.D.W.)

Notes

The authors declare no competing financial interest.

■ ACKNOWLEDGMENTS

The authors are thankful to the EPSRC, the EPSRC National Mass Spectrometry Service Centre (NMSSC) Swansea, the School of Chemistry St. Andrews, and EaStCHEM for support. The author(s) would also like to acknowledge the use of the EPSRC U.K. National Service for Computational Chemistry Software (NSCCS) at Imperial College London in carrying out this work. Calculations were performed using the EaStCHEM Research Computing Facility maintained by Dr. H. Fruchtl and a Silicon Graphics Altix cluster at NSCCS. M.B. wishes to thank EaStCHEM and the University of St. Andrews for support.

■ DEDICATION

Dedicated to Prof. Dr. Wolf-Walther du Mont on the occasion of his 70th birthday.

■ REFERENCES

(1) Balasubramaniyan, V. *Chem. Rev.* **1966**, *66*, 567–641.
(2) Kilian, P.; Knight, F. R.; Woollins, J. D. *Chem.—Eur. J.* **2011**, *17*, 2302–2328.
(3) Kilian, P.; Knight, F. R.; Woollins, J. D. *Coord. Chem. Rev.* **2011**, *255*, 13871–1413.
(4) Brock, C. P.; Dunitz, J. D. *Acta Crystallogr.* **1982**, *B38*, 2218–2228.
(5) (a) Sobczyk, L. *J. Mol. Struct.* **2010**, *972*, 59–63. (b) Llamas-Saiz, A. L.; Foces-Foces, C.; Elguero, J. *J. Mol. Struct.* **1994**, *328*, 297–323. (c) Staab, H. A.; Saupe, T. *Angew. Chem.* **1988**, *100*, 895–909; *Angew. Chem., Int. Ed. Engl.* **1988**, *27*, 865–880.
(6) Kilian, P.; Slawin, A. M. Z.; Woollins, J. D. *Chem.—Eur. J.* **2003**, *9*, 215–222.
(7) Kilian, P.; Philp, D.; Slawin, A. M. Z.; Woollins, J. D. *Eur. J. Inorg. Chem.* **2003**, *2*, 249–254.
(8) Kilian, P.; Slawin, A. M. Z.; Woollins, J. D. *Chem. Commun.* **2003**, 1174–1175.
(9) Wawrzyniak, P.; Fuller, A. L.; Slawin, A. M. Z.; Kilian, P. *Inorg. Chem.* **2009**, *48*, 2500–2506.
(10) Chalmers, B. A.; Bühl, M.; Athukorala Arachige, K. S.; Slawin, A. M. Z.; Kilian, P. *J. Am. Chem. Soc.* **2014**, *136*, 6247–6250.
(11) Hupf, E.; Lork, E.; Mebs, S.; Chęcińska, L.; Beckmann, J. *Organometallics* **2014**, *33*, 7247–7259.
(12) Surgenor, B. A.; Bühl, M.; Slawin, A. M. Z.; Woollins, J. D.; Kilian, P. *Angew. Chem., Int. Ed.* **2012**, *51*, 10150–10153.
(13) Knight, F. R.; Randall, R. A. M.; Roemmele, T. L.; Boer, R. T.; Bode, B. E.; Crawford, L.; Bühl, M.; Slawin, A. M. Z.; Woollins, J. D. *ChemPhysChem* **2013**, *14*, 3199–3203.
(14) Knight, F. R.; Fuller, A. L.; Slawin, A. M. Z.; Woollins, J. D. *Chem.—Eur. J.* **2010**, *16*, 7503–7516.
(15) Knight, F. R.; Fuller, A. L.; Bühl, M.; Slawin, A. M. Z.; Woollins, J. D. *Chem.—Eur. J.* **2010**, *16*, 7617–7634.
(16) Davis, R.; Patel, L. Chapter 5: Chalcogen–Phosphorus (and Heavier Congener) Compounds. In *Handbook of Chalcogen Chemistry: New Perspectives in Sulfur, Selenium and Tellurium,* 2nd ed.; Devillanova, F. A., du Mont, W.-W., Eds.; RSC: Cambridge, U.K., 2013; Vol. *1*.
(17) Corbridge, D. E. C. *Phosphorus World—Chemistry, Biochemistry and Technology;* CRC Press: Boca Raton, FL, 2005, p 747.
(18) Allen, F. H. *Acta Crystallogr.* **2002**, *B58*, 380–388.
(19) Recent examples include (a) Beckmann, J.; Bolsinger, J.; Duthie, A.; Finke, P.; Lork, E.; Lüdtke, C.; Mallow, O.; Mebs, S. *Inorg. Chem.* **2012**, *51*, 12395–12406. (b) Nordheider, A.; Chivers, T.; Schön, O.; Karaghiosoff, K.; Athukorala Arachchige, K. S.; Slawin, A. M. Z.; Woollins, J. D. *Chem.—Eur. J.* **2014**, *20*, 704–712. (c) Nordheider, A.; Chivers, T.; Thirumoorthi, R.; Athukorala Arachchige, K. S.; Slawin, A. M. Z.; Woollins, J. D.; Vargas-Baca, I. *Dalton Trans.* **2013**, *42*, 3291–3294.
(20) (a) Dibromoacenaphthene: Tanaka, N.; Kasai, T. *Bull. Chem. Soc. Jpn.* **1981**, *54*, 3020–3025. (b) $(^iPr)_2$P–Ace–Br): Wawrzyniak, P.; Fuller, A. L.; Slawin, A. M. Z.; Kilian, P. *Inorg. Chem.* **2009**, *48*, 2500–2506. (c) $(Ph_2P$–Ace–Br): Beckmann, J.; Do, T. G.; Grabowsky, S.; Hupf, E.; Lork, E.; Mebs, S. *Z. Anorg. Allg. Chem.* **2013**, *639*, 2233–2249.
(21) No decomposition of the solids was observed after three days; no oxidation of the P^{III} centers was observed.
(22) Bondi, A. *J. Phys. Chem.* **1964**, *68*, 441–452.
(23) Dutton, J. L.; Ragogna, P. J. *Inorg. Chem.* **2009**, *48*, 1722–1730.
(24) Ritch, J. S.; Chivers, T.; Eisler, D. J.; Tuononen, H. M. *Chem.—Eur. J.* **2007**, *13*, 4643–4653.
(25) Aschenbach, L. K.; Knight, F. R.; Randall, R. A. M.; Cordes, D. B.; Baggott, A.; Bühl, M.; Slawin, A. M. Z.; Woollins, J. D. *Dalton Trans.* **2012**, 3141–3153.
(26) Wawrzyniak, P.; Fuller, A. L.; Slawin, A. M. Z.; Kilian, P. *Inorg. Chem.* **2009**, *48*, 2500–2506.
(27) Chalmers, B. A.; Athukorala Arachchige, K. S.; Prentis, J. K. D.; Knight, F. R.; Kilian, P.; Slawin, A. M. Z.; Woollins, J. D. *Inorg. Chem.* **2014**, *53*, 8795–8808.

DOI: 10.1021/ic503056z
Inorg. Chem. 2015, 54, 2435–2446

(28) The details of the calculations are shown in the Supporting Information. The J(P,Te) values were calculated to have a negative prefix, where the experimental values are shown as absolute values.
(29) Details of the solid-state NMR experiments can be found in the Supporting Information.
(30) Bühl, M.; Knight, F. R.; Krístková, A.; Malkin Ondík, I.; Malkina, O. L.; Randall, R. A. M.; Slawin, A. M. Z.; Woollins, J. D. *Angew. Chem., Int. Ed.* **2013**, *52*, 2495−2498.
(31) Mallory, F. B. *J. Am. Chem. Soc.* **1973**, *95*, 7747−7752.
(32) Hierso, J.-C. *Chem. Rev.* **2014**, *114*, 4838−4867.
(33) All coupling constants from experimental data are reported as absolute values. However, the calculated ^{1}J(P,Te) or ^{1}J(Te,Se) were shown to be negative.
(34) For technical reasons 6-311G(d) instead of 6-311+G(d) basis had to be used to plot the NBOs (single point calculation on the optimized geometries). For NBO analysis see: Reed, A. E.; Curtiss, F.; Weinhold, L. A. F. *Chem. Rev.* **1988**, *88*, 899−926.
(35) Wiberg, K. B. *Tetrahedron* **1968**, *24*, 1083−1096.
(36) Horn, E.; Nakahodo, T.; Fukurawa, N. *Z. Kristallogr.—New Cryst. Struct.* **2000**, *215*, 23−25.
(37) Bader, R. F. W.: *Atoms in Molecules. A Quantum Theory;* Oxford University Press: New York, 1990.
(38) (a) Kohout, M. *Int. J. Quantum Chem.* **2004**, *97*, 651−658. (b) Kohout, M.; Wagner, F. R.; Grin, Y. *Theor. Chem. Acc.* **2008**, *119*, 413−420.
(39) (a) Raub, S.; Jansen, G. *Theor. Chem. Acc.* **2001**, *106*, 223−232. (b) Vidal, I.; Melchor, S.; Dobado, J. A. *J. Phys. Chem. A* **2005**, *109*, 7500−7508.
(40) Eisler, D. J.; Robertson, S. D.; Chivers, T. *Can. J. Chem.* **2009**, *87*, 39−46.
(41) Copsey, M. C.; Panneerselvam, A.; Afzaal, M.; Chivers, T.; O'Brien, P. *Dalton Trans.* **2007**, 1528−1538.
(42) Hierso, J.-C.; Fihri, A.; Ivanov, V. V.; Hanquet, B.; Pirio, N.; Donnadieu, B.; Rebière, B.; Amardeil, R.; Meunier, P. *J. Am. Chem. Soc.* **2004**, *126*, 11077−11087.
(43) Spin-spin couplings involving Pt have been shown to be very sensitive to the density functional and, in particular, solvation Sutter, K.; Truflandier, L. A.; Autschbach, J. *ChemPhysChem* **2011**, *12*, 1448−1455 a side issue, which we did not explore further.

DOI: 10.1021/ic503056z
Inorg. Chem. 2015, 54, 2435−2446